Acceptance Studies for the FPD

Jorge Barreto
Instituto de Física
Universidade Federal do Rio de Janeiro, UFRJ - RJ - Brazil

and

José Montanha *
Instituto de Física
Universidade Estadual de Campinas, UNICAMP - SP - Brazil

10th November 2000

Abstract

A study of the geometrical and total acceptance for the FPD quadrupole and dipole detectors is presented. It is found that, for quadrupole detectors, the choice of parameterization for the t dependence can have a major effect in the value of the integrated acceptance, although it does not change the shape of its ξ dependence, or the minimum values of t that fire the detectors. For dipole detectors such choice is less important, since those detectors cover mostly the low t region.

1 Introduction

In this note we present the results for the acceptance studies concerning the Forward Proton Detector (FPD) spectrometers, using the new tracking algorithm developed by the FPD group [1], which incorporates the Tevatron lattice modifications due to the removal of the D0Q1 low beta quadrupole. Preliminary acceptance studies for the Forward Proton Detector were performed using the MAD and BEAMLINE (C++) codes, provided by the Beam Division [2], which can be found in ref. [3].

The focus of this note is in both the quadrupole and dipole spectrometers, for which the geometrical and total acceptance are presented as a function of the momentum of the scattered proton. In section 2 we describe the variables relevant to the process of hadronic difraction. Section 3 accounts for the acceptance calculation method . The results for the quadrupoles are presented in section 4 and for the dipole in section 5. In section 6 we drawn some final remarks.

* Work supported by Fundação de Amparo à Pesquisa do Estado de São Paulo - Proc. 99/01236-9

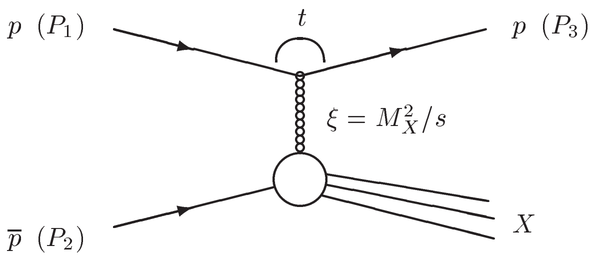

Figure 1: Kinematics for the single diffractive reaction $p\,\overline{p} \;\rightarrow\; p\,X$.

2 Kinematics, Cross Sections and Slopes

In a single diffractive (SD) reaction at Tevatron, a proton of four-momentum P_1 interacts with an anti-proton of four-momentum P_2, with one of the incoming particles been detected in the final state, with a four-momentum P_3. The kinematics for the reaction is given in figure 1. Here $s = (P_1 + P_2)^2$ is the square of the center of mass energy of the collision; $t = (P_1 - P_3)^2$ is the four-momentum transferred squared, and $M_X^2 = (P_1 + P_2 - P_3)^2$ is the squared mass of the system X which, for diffractive events, carries the same quantum numbers of particle P_2.

In an elastic scattering ($p\overline{p} \;\rightarrow\; p\overline{p}$), t is only a function of the center of mass scattering angle θ between the incoming and outgoing particles, since the absolute value of the momentum $\vec{k}$ of the particles does not change. In this case, the expression for t is

$$t = (P_1 - P_3)^2 = -4k^2 sin^2(\theta/2) \sim -p_t^2, \tag{1}$$

where p_t^2 is the transverse momentum squared of the elastically scattered particle. According to this equation t is negative and, to avoid misunderstandings, in the future we will refer to its absolute value, $|t|$.

In a single diffractive scattering one of the incoming particles looses a fraction $\xi = M_X^2/s = 1 - (P_3/P_1)$ of its momentum, with $\xi \leq 0.15$ due to the coherence condition imposed over hadronic diffraction [4]. For such range of ξ values, we can write

$$t = (P_1 - P_3)^2 \sim -\frac{p_t^2 + m_p^2\,\xi^2}{1-\xi}; \tag{2}$$

where m_p is the mass of the outgoing proton. According to this result, the minimum value of $|t|$ is now a function of ξ;

$$|t_{min}| = \frac{m_p^2\,\xi^2}{1-\xi}. \tag{3}$$

For the FPD quadrupole spectrometers, such lower bound on $|t|$ is of no importance, since for $\xi \sim 0.15 \rightarrow |t_{min}| \sim 0.023\ GeV^2$, and the experimental configuration of the

FPD imposes a minimum value upon the $|t|$ acceptance of the quadrupole spectrometers which is, already, much higher than this one. However, such constraint will show its effect over the dipole spectrometer, since that device has good acceptance for $|t| \rightarrow 0$ at high ξ.

An important ingredient in the acceptance calculation is the expression for the differential cross section, $d\sigma/dt$. A suitable expression for the t dependence of the SD cross section, at small $|t|$ values ($|t| << 1\,GeV^2$) and at fixed ξ, is given by [4]:

$$\frac{d\sigma}{dt} \approx A\, e^{-b(\xi)\,|t|}, \tag{4}$$

where $b(\xi)$ is the slope, defined as:

$$b(\xi) = \frac{d}{dt}\; ln\; \frac{d\sigma}{dt}|_{t=0}. \tag{5}$$

Following Regge phenomenology, $b(\xi)$ can be parameterized by the expression:

$$b(\xi) = b_o^{SD} + 2\alpha'\; ln(\xi^{-1}) \tag{6}$$

where α' and b_o^{SD} are extracted from fits to experimental data.

From elastic scattering data, it is well known that $\alpha' = 0.25\; GeV^{-2}$, and from the standard approach to single diffraction phenomenology, we can assume b_o^{SD} as half the value of the elastic one, b_o^{el}, so that we have $b_o^{SD} \sim b_o^{el}/2 = 4.6\; GeV^{-2}$, and the standard slope then reads:

$$b(\xi) = 4.6 + 0.5\, ln(\xi^{-1}). \tag{7}$$

The CDF Collab. [5] fitted their data on $p\,\overline{p}$ single diffractive dissociation at $\sqrt{s} = 1800\; GeV$ with an exponential cross, section according to eq. (4), and with a slope parameter following eq. (6). From that they found

$$b(\xi) = (4.2 \pm 0.5) + 0.5\, ln(\xi^{-1}), \tag{8}$$

which pretty much agrees with the standard expression (7).

However, it should be noted that CDF uses only dipole roman pots, therefore their acceptance is concentrated in the small $|t|$ region, where eq. (4) is supposed to give a good description of the data. For higher values of $|t|$ ($> 0.1\; GeV^2$), a more appropriate expression for describing the t dependence is given by [6]:

$$\frac{d\sigma}{dt} \approx A\, F_1^2(t)\, e^{-0.5 ln(\xi^{-1})\,|t|} \tag{9}$$

where the function F_1, also known as the Dirac form factor, is defined as:

$$F_1(t) = \frac{4m_p^2 + 2.8\,|t|}{4m_p^2 + |t|}\,\frac{1}{(1 + |t|/0.71)^2}. \tag{10}$$

Using expression (9) in the definition of slope, eq. (5), we just recover the standard slope, eq. (7):

$$b^{F1}(\xi) = \frac{d}{dt}\; ln\; A\, F_1^2(t)\, e^{-0.5 ln(\xi^{-1})\,|t|} \approx 4.6 + 0.5\; ln(\xi^{-1}). \tag{11}$$

3 Acceptance Calculation

The acceptance, or geometrical efficiency, is the fraction of the scattered particles which are geometrically intercepted by the detector [7]. It depends on the geometrical configuration of the detector, and on the differential cross section of the scattered particles.

The differential acceptance for a detector with cylindrical symmetry as a function of t and of the azimuthal angle ϕ, appropriately normalized so that the full integrated acceptance is equal to unity, is given by

$$a(\xi, t, \phi)\ dt\ d\phi = \frac{1}{\sigma(\xi)} \frac{d\sigma}{dt}\ dt\ da_\phi; \tag{12}$$

where

$$da_\phi = \frac{d\phi}{2\ \pi} \tag{13}$$

is the differential geometric acceptance, normalized so that its integral from 0 to 2π is equal to unity, and

$$\sigma(\xi) = \int_0^\infty \frac{d\sigma}{dt}(\xi, |t|)\ dt \tag{14}$$

provides the appropriate normalization for the t-integrated acceptance. Indeed, for a differential cross section given by expression (4), we have

$$\sigma(\xi) = \int_0^\infty \frac{d\sigma}{dt}(\xi, |t|)\ dt = \frac{A}{b(\xi)}. \tag{15}$$

To obtain the total acceptance $a(\xi)$, we have to integrate eq. (12) over $|t|$ and ϕ values lying inside the active area of the detector. In fact what is actually done is a sum over values of $|t|$ and ϕ which correspond to valid tracks for the FPD, i.e., there must be a valid hit in both horizontal or vertical quadrupole detectors at pot stations P1 and P2, or A1 and A2, or at the horizontal dipole detectors at pot stations D1 and D2. It is also imposed that the track trajectory, from the interaction point at the center of the DØ detector to the pot position, must lies inside the beam pipe, which has a inner radius of 35 mm, with an aperture of 25 mm at the separators.

4 Results for the Quadrupoles

All the results presented in this section were evaluated for the scattered proton side of the detector. The anti-proton side corresponds to a rotation of $\pi/2$ around the beam axis, which effectively means to change places between the vertical and horizontal detectors, so that the vertical anti-proton spectrometer displays the same results as the horizontal proton spectrometer, etc. The whole analysis assumes an 8σ pot displacement from the beam.

The geometrical configuration of a FPD quadrupole pot station is shown in figure 2. The azimuthal angle ϕ, for a fixed $|t|$ and ξ, runs from 0 to 2π, producing an elliptical pattern such the one displayed in the figure.

The minimum value of $|t|$ that establishes a threshold for the acceptance, as a function of ξ, is presented in figure 3. The minimum $|t|$ accepted by both vertical and horizontal spectrometers is $0.58\ GeV^2$ as $\xi \to 0$, with the minimum value for the horizontal spectrometers increasing up to $4.16\ GeV^2$ for $\xi = 0.085$, where it becomes iqual to the maximum $|t|$ value for these spectrometers. The vertical detectors have a more stable minimum that changes only to $0.75\ GeV^2$ as $\xi \to 0.1$, and a maximum accepted $|t|$ that lays around $2.2\ GeV^2$.

The geometric acceptance is the effective angular area covered by the detectors. It can be obtained by integrating eq. (13), for a fixed value of $|t|$ and ξ, over the active area of the vertical and horizontal spectrometers. The maximum acceptance so obtained is 79% at $|t| = 1.29\ GeV^2$. Figure 4 displays the geometric acceptance as a function of ξ and $|t|$.

The total acceptance corresponds to integrate eq. (12) over ϕ and $|t|$ values inside the active area of the spectrometers. According to eq. (12), it is not a function of the geometry of the detectors only, as in the case of the geometric acceptance, but depends also on the choice of parameterization for the differential cross section. For that we have two parameterizations, eq. (4) and eq. (9), as discussed in section 2, with a choice of two slope parameters for the former, the standard slope (eq. 7) and the CDF one (eq. 8) . In table 1 we present the results obtained for each of these choices.

	$\xi = 0.002$	$\xi = 0.01$	$\xi = 0.02$	$\xi = 0.03$	$\xi = 0.05$
Stand.	0.53	0.69	0.66	0.59	0.51
CDF	0.68	0.90	0.87	0.79	0.67
$F_1^2(t)$	1.63	2.40	2.55	2.48	2.24

Table 1: Results for the total acceptance (%) vs. ξ at 8σ pot locations, using different $|t|$ dependences for the diffractive cross section.

Eq. (9) gives an acceptance result that is 3 times bigger than both the standard and CDF results, for all ξ values. That is expected, as discussed before, from the fast drop of the differential cross section coming from the exponential behavior of eq. (4) with $|t|$, for high $|t|$ values. The choice of the $|t|$ dependence does not affect, however, the shape of the acceptance at a function of ξ, displayed in figure 5, which is basically the same for all choices of cross section and slope.

Another important factor affecting the total acceptance is the pot position relative to the center of the beam. Table 2 presents the 8σ position values for the horizontal and vertical pots that we have been using in this analysis, and figure 6 presents the variation of the total acceptance, for $\xi = 0.02$, with the pot position, in units of σ.

	POT P1 (mm)	POT P2 (mm)
UP	14.5704	12.1892
DOWN	-14.5704	-12.2291
OUT	8.1583	6.2655
IN	-8.1583	-6.4772

Table 2: 8σ pot positions relative to the center of the beam.

5 Results for the Dipoles

Dipole spectrometers are placed at the horizontal plane of the anti-proton arm, so they tag the diffractively scattered anti-proton only. An anti-proton is considered to be accepted by the dipole spectrometer if it passes through the active area of both detectors D1 and D2, while remaining within the limiting aperture of the beam pipe throughout its entire trajectory. The elliptic trajectory of the diffractivelly scattered anti-protons, relative to the dipole detectors, are shown in figure 7 for 8σ pot displacement from the beam.

Figure 8 shows the geometric acceptance for the dipole spectrometer in bins of ξ and t. In order to be true to the kinematics, we imposed the $|t_{min}|$ constraint, given by eq. (3). The main effect of such constraint is to introduce a ξ dependent lower bound for $|t|$, that prevents it from going to zero for $\xi > 0$. However, since we are concerned with small ξ values, $|t_{min}|$ is quite small and the whole effect cannot be noticed in figure 8.

We found that 100% geometric acceptance can be achieved for bins in the range $0.027 \leq \xi \leq 0.068$, with the maximum $|t|$ interval for 100% acceptance been $0.0021 \leq |t| \leq 1.73\, GeV^2$ at $\xi = 0.048$.

The total acceptance (integrated over ϕ and $|t|$) as a function of ξ is presented in figure 9, for 8σ pot position. The ξ range covered by the detectors goes from $\xi \approx 0$ up to $\xi \approx 0.075$, with an acceptance bigger than 90% in the range $0.031 \leq \xi \leq 0.065$, assuming the exponential parameterization for the cross section with the standard slope, eq. (7). No significant difference was found in the shape of the curve using the CDF slope or the Dirac form factor.

Table 3 presents some numerical values for the total acceptance at several ξ values, taken at 8σ pot displacement. For each ξ, we explore the different $|t|$ parameterizations of $d\sigma/dt$, in order to test the sensitivity of the acceptance upon the choice of form factor, as in the case of the quadrupole spectrometers. Again we take the exponential parameterization for the differential cross section, given by eq. (4), with the standard slope, eq. (7), or the CDF one, eq. (8), and also eq. (9) with the Dirac form factor, given by eq. (10).

As expected for high ξ values, all $|t|$ parameterizations give close results for the total acceptance, the main difference lying in the small ξ region. Indeed, for $\xi = 0.001$, the Dirac form factor parameterization gives an acceptance twice as high as the ones from the standard and CDF expressions. However, as ξ grows, such difference becomes smaller and, for $\xi = 0.03$, all three results basically agree with each other. That happens, basically, because of the excellent small $|t|$ acceptance of the spectrometer for all but the smaller ξ values, as shown in figure (8).

	$\xi = 0.001$	$\xi = 0.005$	$\xi = 0.01$	$\xi = 0.03$	$\xi = 0.05$
Stad.	0.16	0.98	4.55	88.71	99.99
CDF	0.21	1.16	5.05	87.93	99.99
$F_1^2(t)$	0.47	1.98	6.59	85.84	99.87

Table 3: Results for the total acceptance (in %) vs. ξ at 8σ pot locations, using different $|t|$ dependences for the diffractive differential cross section.

6 Conclusions

We performed an analysis of the acceptance for the FPD quadrupole and dipole spectrometers using the new Tevatron lattice. For an 8σ pot position we found, for the quadrupole spectrometers, a maximum geometrical acceptance of approximately 79% at $|t| = 1.29\,GeV^2$, and a total acceptance value that stays around 2.4% for $\xi > 0.01$. For the dipole spectrometer, we have a maximum geometrical acceptance of 100%, over the range $0.027 \leq \xi \leq 0.068$, for small $|t|$ values. A maximum total acceptance of 100% in obtained at $\xi = 0.048$, over the range $0.0021 \leq |t| \leq 1.73\,GeV^2$, and a total acceptance between $90\xi \leq 0.065$.

It was found that, for the quadrupole spectrometers, the choice for the expression describing the differential cross section has a major impact in the amount of the calculated acceptance. An exponential parameterization underestimates the high $|t|$ contribution, which can be more correctly described using the $F_1(t)$, or Dirac, form factor. It is worth to note that such expression is a standard parameterization used in Monte Carlo diffractive generators such as Pompyt. It is also worth to mention that the dipole acceptance is much less sensitive to the choice of the $|t|$ dependence of $d\sigma/dt$ since, at small $|t|$, the Dirac form factor presents a behavior similar to the standard slope, as described in eq. (11).

7 Acknowledgements

Jorge Barreto is thankful to Fundação de Amparo à Pesquisa do Estado do Rio de Janeiro for partially support this work. José Montanha wishes to gratefully acknowledge the fellowship provided by Fundação de Amparo à Pesquisa do Estado de São Paulo - FAPESP.

References

[1] J. Barreto and A. Drozdhin, Reconstructing Track Trajectories for the FPD; FPD memo (www.if.ufrj.br/ barreto/fpd.html).

[2] Tracking program provided by Michael Martens and L. Michelotti, Fermilab Beam Division.

[3] A Forward Proton Detector at D0; A. Brandt et al., FERMILAB-Pub-97/377.

[4] K. Goulianos: Phys. Rep. **101** (1983) 169.

[5] F. Abe *et al.*, The CDF Collab.: Phys. Rev. D **50** (1994) 5535, 5550.

[6] K. Goulianos and J. Montanha; Phys. Rev. D **59** (1999) pp. 1-13 (114017)

[7] W. R. Leo; Techniques for Nuclear and Particle Physics Experiments. Springer-Verlag 1994.

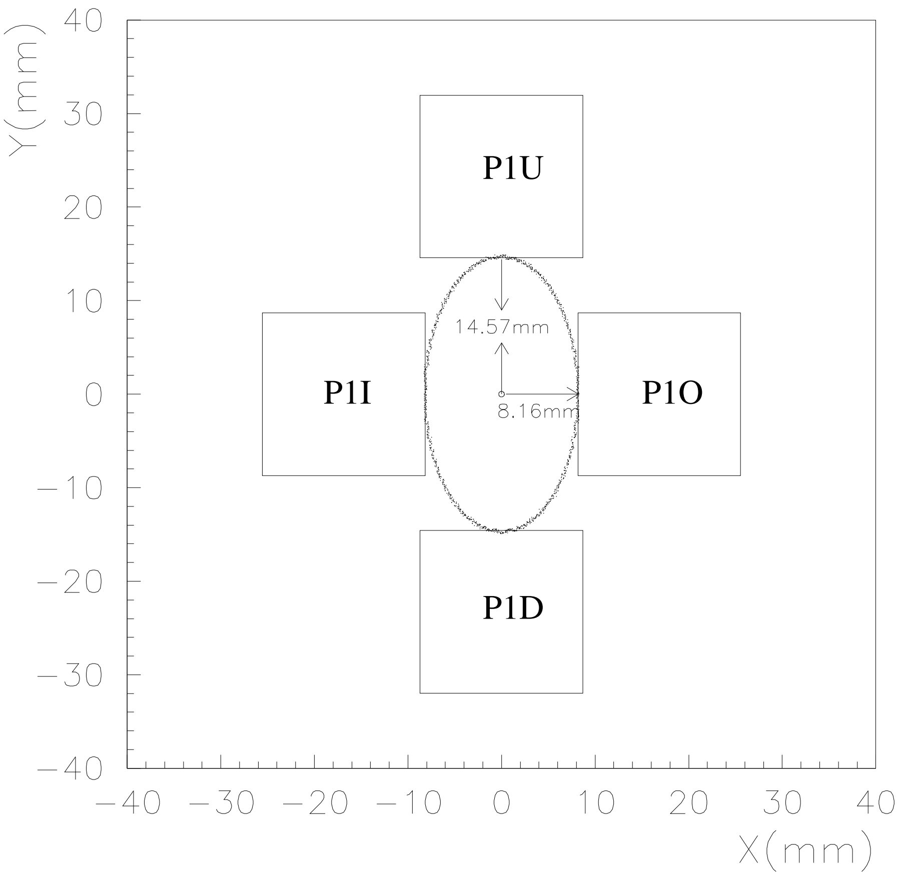

Figure 2: Cross section of pot station P1, showing the spectrometers position relative to the beam, at 8σ.

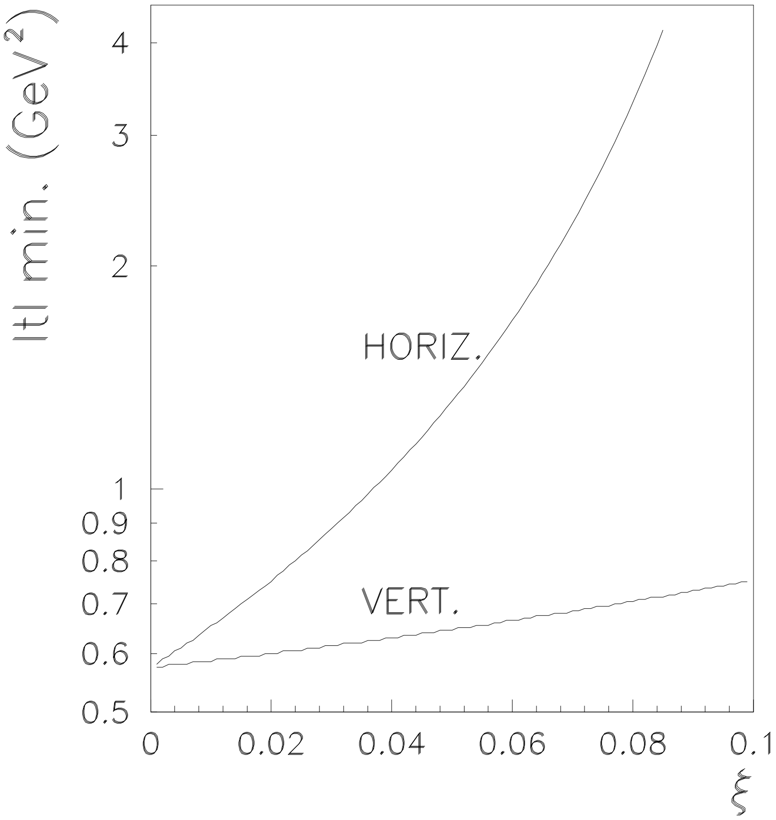

Figure 3: Minimum $|t|$ values for the quadrupole detectors as a function of ξ.

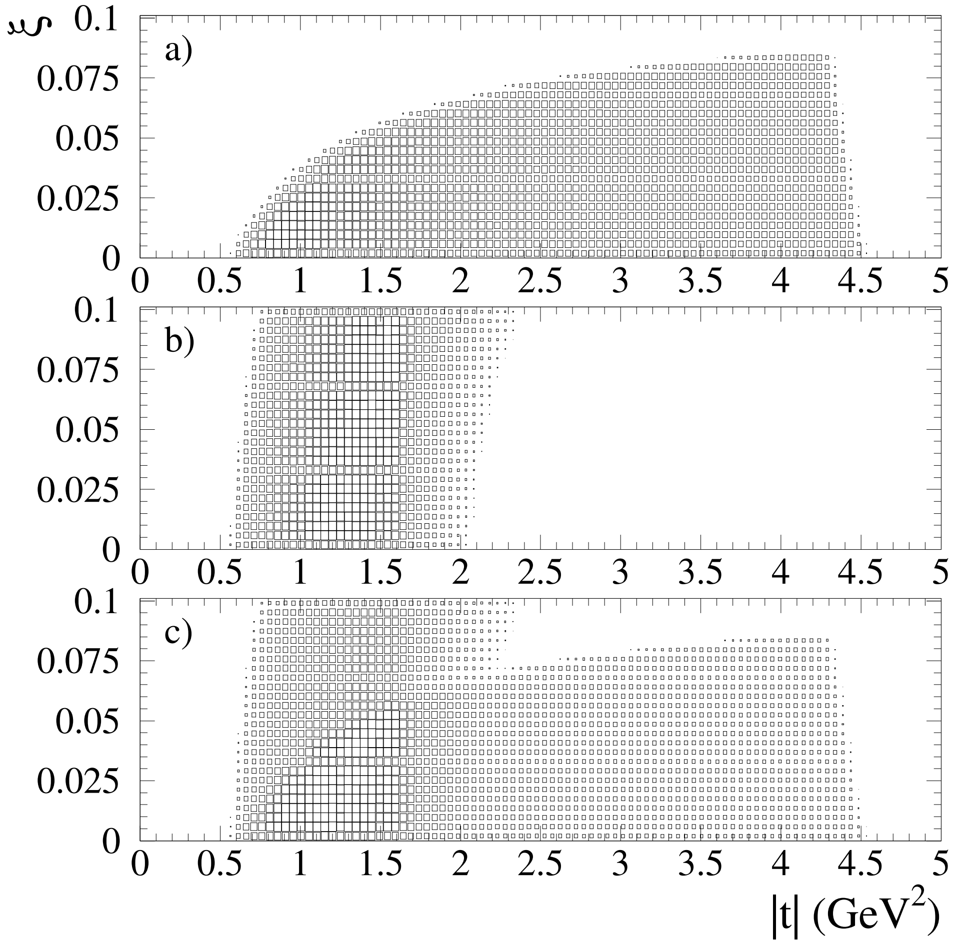

Figure 4: Geometric acceptance for a) horizontal; b) vertical and c) sum of both pots in bins of ξ and $|t|$. The size of the box is proportional to the amount of acceptance

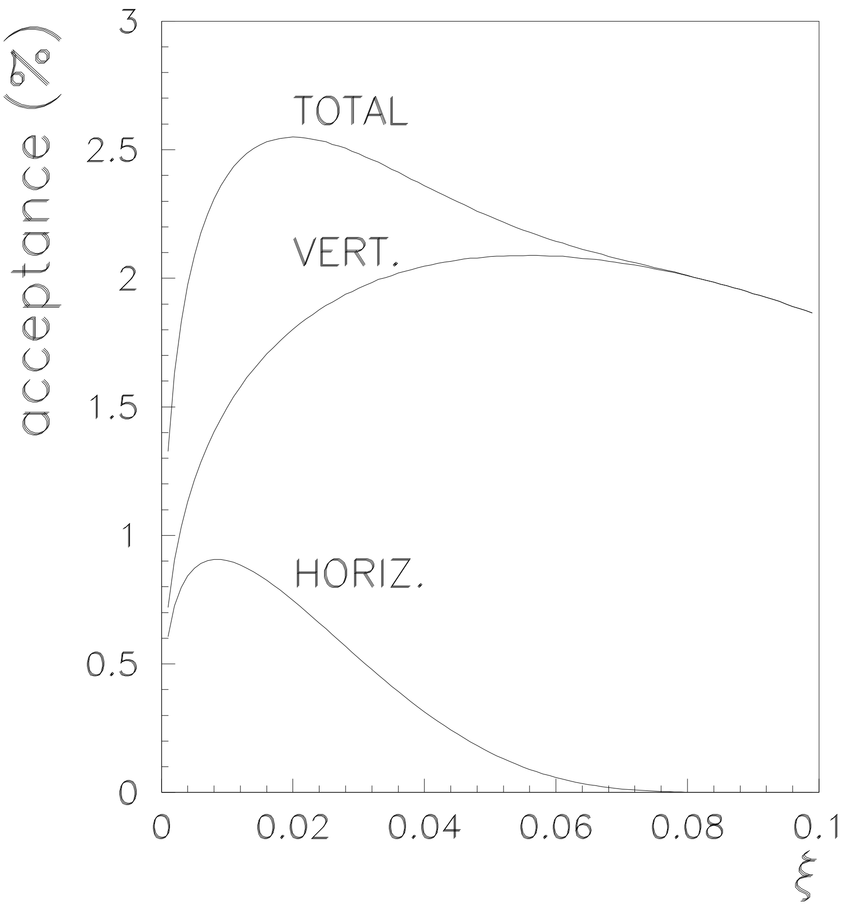

Figure 5: Integrated acceptance (in %) as a function of ξ, for the horizontal and vertical pots. The total curve represent the sum of both contributions. The results here were calculated with the $F_1^2(t)$ cross section parameterization, eq. (9).

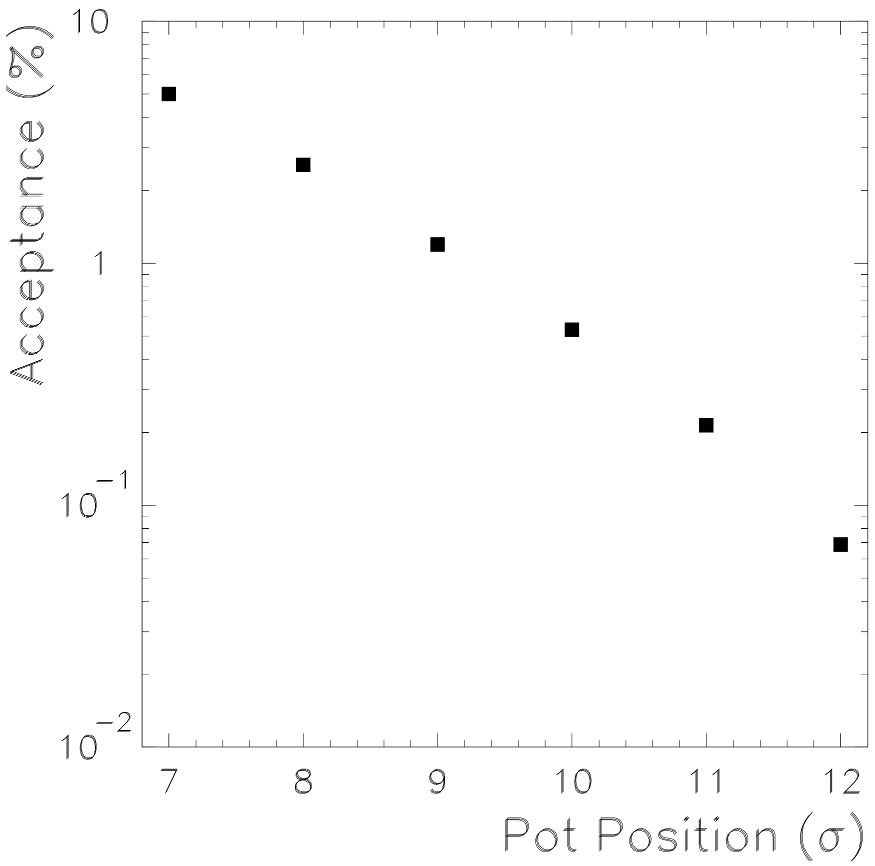

Figure 6: Total integrated acceptance (in %) as a function of the pot position, in units of σ.

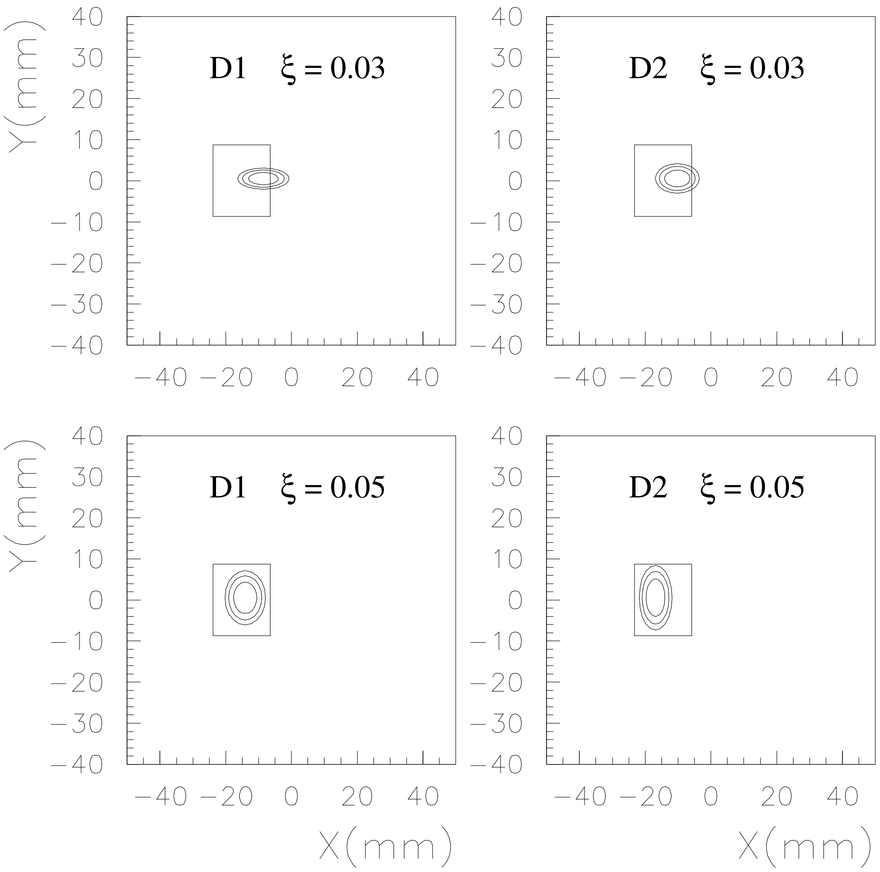

Figure 7: The x and y displacement at the $D1$ and $D2$ dipole pot locations are shown, as contours of constant $|t|$, for $|t| = 0.5,\ 1.0$, and $1.5\,GeV^2$, for 8σ displacement. Top plots, $\xi = 0.03$; bottom plots, $\xi = 0.05$.

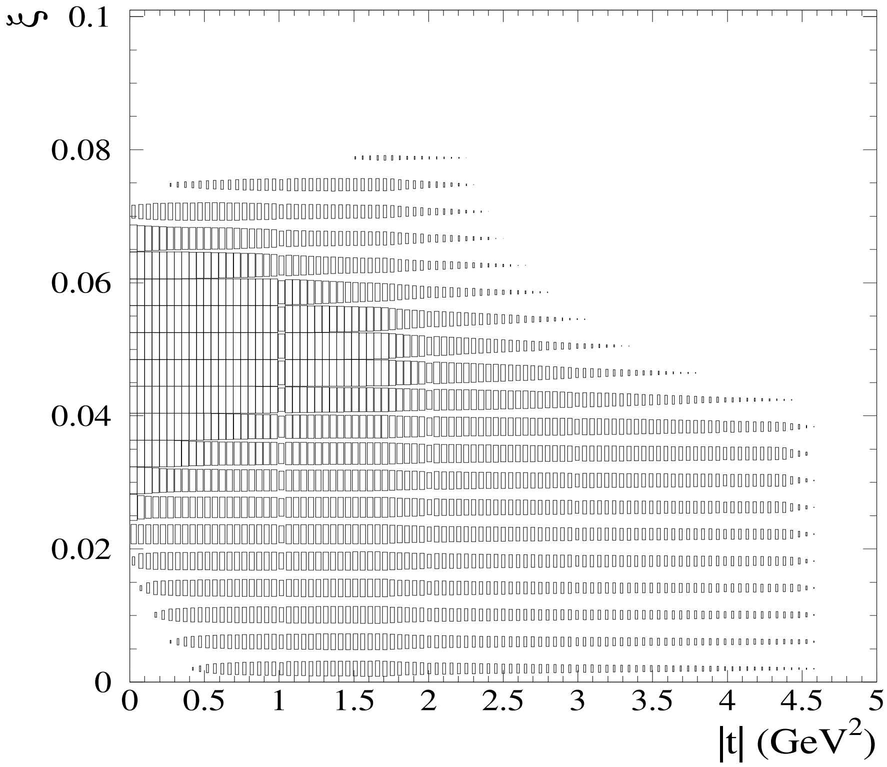

Figure 8: Geometric acceptance in bins of ξ and $|t|$ for the dipole spectrometer, with the detectors at 8σ displacement. The acceptance in each bin is proportional to the size of the box, with the largest box representing 100% acceptance.

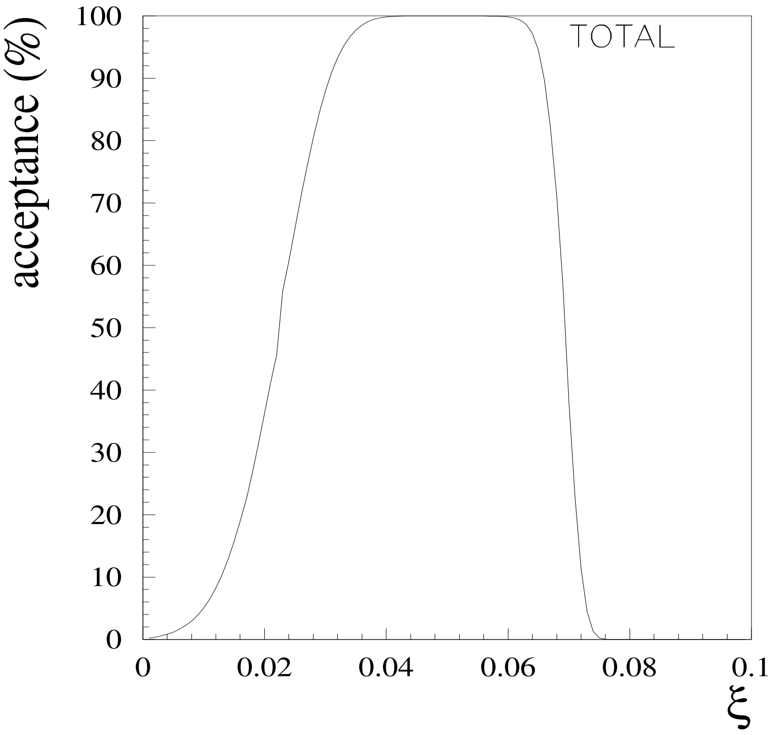

Figure 9: Total acceptance (integrated over ϕ and $|t|$) as a function of ξ at 8σ pot displacement.